Biosensors and Bioelectronics 140 (2019) 111338

Contents lists available at ScienceDirect

Biosensors and Bioelectronics

journal homepage: www.elsevier.com/locate/bios

Cell-line characterization by infrared-induced pyroelectric effect

Salvatore A. Pullano[a,*,1], Marta Greco[a,1], Domenica M. Corigliano[a], Daniela. P. Foti[a], A. Brunetti[a], Antonino S. Fiorillo[a]

[a] Department of Health Sciences, University "Magna Græcia" of Catanzaro, 88100, Catanzaro, Italy

ARTICLE INFO

Keywords:
Pyroelectric sensor
Biological cell characterization
Thin film devices
Cellular biophysics
Thermal factors
Sensor phenomena and characterization
Counting circuits

ABSTRACT

Evaluation of cellular thermodynamics has recently received a high interest because of its implication in many mechanisms related with function, structure and health of cells. Recent literature reported significant efforts to provide affordable intracellular thermal components of absorption, such as thermal conductivity, to overcome the lack of experimental data.

Herein, we provide lines of evidence towards the fabrication of an electronic system, using a rapid thermoelectric technique based on infrared–induced pyroelectric effect for *in-vitro* cell model characterization.

Results demonstrated that the assessment of the average single cell thermal conductivity, sample concentration, and information on cell viability is possible over a wide concentration range. The proposed electronic system establishes a different analysis paradigm if compared to those reported in the literature, with consistent results, demonstrating that the adopted technique can provide cell-specific information and knowledge, closely linked to cell viability and its vital functions.

1. Introduction

In-vivo and *in-vitro* applications often require repetitive steps of cell characterization (Green et al., 2015; Antoni et al., 2015). Among the main standard procedures, it is important to mention the evaluation of concentration, proliferation and viability of cells, to ensure reproducibility and accuracy of biological data. (Ongena et al., 2010; Ramirez et al., 2016). The unbiased cell number estimation is routinely performed by manual hemocytometer with inherent errors higher than 10% (Peniuk et al., 2015). Automatic devices based on light dispersion and bio-impedance (Takahashi, 2018; Xu et al., 2016; Yu et al., 2005), represent the gold standard for cell counting and sorting to provide dimensional and functional information on the sample (Saeys et al., 2016; Adan et al., 2017). Among functional information, cell viability is a key parameter traditionally investigated by colorimetric assays (e.g. neutral red uptake, trypan blue) commonly used to explore cytotoxicity, cytopathogenicity, and immunotoxicity. The use of dyes as markers of vital status should be, however, considered with caution, since false negative or positive results, such as the maintenance of membrane integrity in cells with impaired viability, or the maintenance of cell viability in the presence of increased membrane permeability, may also occur (Repetto et al., 2008; Strober, 2015; Nicoletti et al., 1991; Riccardi and Nicoletti, 2006; Tran et al., 2011).

Among recently investigated and commercialized label-free techniques, electric impedance sensing is widely accepted to assess cellular status (Ongena et al., 2010; Zhang et al., 2018; Chou et al., 2018; García-Sánchez et al., 2018). A growing interest in the thermodynamics of cells evidenced that thermal monitoring has the potential to provide interesting insights on gene expression and tumor metabolism (Vreugdenburg et al., 2013; Kucsko et al., 2013, Yasuhiro et al., 2009). The cell thermodynamics is ruled by the physical properties of the cell components (e.g. mitochondria, and other cytosolic organelles), through specialized temperature-sensitive receptors which affect metabolic and enzymatic reactions, and consequently cellular viability (Sharkey and Schrader, 2006; Willmer et al., 2009; Wang et al., 2011). Significant efforts have been performed in this field by the miniaturization of thermal probe (Kucsko et al., 2013) or by using different calorimetric approaches (Park et al., 2013, 2016; Vega et al., 2015). Preliminary results evidenced that a cost-effective electronics and a simple post-processing can be employed jointly with thermoelectric conversion on cell suspensions, indicating a detectable signal contribution of thermal nature (Pullano et al. 2017a, 2019).

In the attempt to gain thermodynamic and thermophysical data on biological samples and to improve the throughput, herein we propose a thermoelectric approach based on infrared (IR)-induced pyroelectric effect for the characterization of low-volume cellular suspensions. The

* Corresponding author.
E-mail address: pullano@unicz.it (S.A. Pullano).
[1] Salvatore A. Pullano and Marta Greco contributed equally to this manuscript.

https://doi.org/10.1016/j.bios.2019.111338
Received 4 March 2019; Received in revised form 13 May 2019; Accepted 17 May 2019
Available online 21 May 2019
0956-5663/

sensor is composed by a thin ferroelectric film made of Polyvinylidene-Fluoride (PVDF) illuminated with IR radiation to periodically induce a pyroelectric response. Four representative *in-vitro* models from distinct tissues (hepatocytes, T lymphocytes, prostate cancer cells and retinal pigment epithelium cells) were investigated under different test conditions. The correlation between induced pyroelectric response and a thermal model allowed to retrieve a set of information of thermoelectric nature, including cell concentration, average single cell thermal conductivity and assessment of cell viability.

Results evidenced how the magnitude of the pyroelectric response increases with sample concentration with a high linearity. At very low concentrations, the differences in thermoelectric conversion were mostly influenced by the surrounding culture medium, leading to reduced linearity. Impaired cell viability by induced necrosis evidenced no output variations even if the sample concentration was significantly increased in the absence of thermodynamic cellular activity. Single cell average thermal conductivity has been evaluated to be characteristics of a specific *in-vitro* model and influenced by its health status. At a given viability, results highlighted that thermal conductivity is characteristic of the specific *in-vitro* model considered. Interesting differences have been observed in Arpe 19 cells, which are specialized pigmented cells that absorb visible light. Finally, the contribution of organelles and cytoplasm on the thermal conductivity have been investigated by modulating HepG2 mitochondrial activity and by inducing apoptotic program (Anson and Chivers, 1989). We found that cytoplasm greatly affects thermal conductivity with respect to mitochondrial activity. Another interesting aspect is that, despite the integrity of the membrane, apoptosis induced by metformin, a commonly used insulin-sensitizer with pleiotropic effects (Schulten, 2018) upregulates the thermal conductivity of the single cell, probably because of the role of AMP-activated protein kinase (AMPK) in the restriction of energy consumption (Sun et al., 2016).

In comparison with a pure calorimetric approach, the thermoelectric conversion provided consistent results, together with an easier and convenient approach for high-throughput evaluation of cell status. From the technological point of view, we demonstrated that a device, designed to be as minimal as possible to reduce the handling of the sample, avoiding fluidic/microfluidic components and complex electronic interface, can provide reliable results on different cell populations by exploiting the use of pyroelectric effects. As far as cell characterization is concerned, the thermoelectric approach establishes a different analysis paradigm, by testing high volume of different cell lines from different sources and providing a suitable cell-specific set of information.

2. Materials and methods

2.1. Cell cultures

In this work, the following human cell lines were used as cellular models: HepG2 hepatocellular carcinoma cells (Iiritano et al., 2012), Jurkat immortalized T lymphocytes (Brunetti et al., 1996), LNCaP prostate adenocarcinoma cells (Horoszewicz et al., 1983), and Arpe19 retinal pigment epithelium cells (Chiefari et al., 2016). HepG2, Jurkat and LNCaP cell lines were maintained in RPMI 1640 medium, while Arpe 19 cells were cultured in DMEM F:12. Culture media were supplemented with 2 mmol/l L-glutamine, 50 IU/ml penicillin, 50 μg/ml streptomycin, and 10% fetal bovine serum. All cell lines were maintained at 37 °C in a humidified 5% CO_2 atmosphere. All cellular models were characterized in terms of average diameter (HepG2 = 29 μm, Jurkat = 22 μm, LNCaP = 25 μm, and Arpe 19 = 33 μm) through a digital microscope (Nikon Digital camera microscope.

2.2. Cell characterization and viability

Necrosis and apoptosis were assessed by a cytofluorimetric assay (FITC Annexin V Apoptosis Detection Kit I – BD Biosciences) as indicated by the manufacturer. Briefly, after 2 washes with cold phosphate buffered saline (PBS), cells were resuspended in 1X Annexin V Binding Buffer 1X (0.1 M Hepes/NaOH (pH 7.4), 1.4 M NaCl, 25 mM $CaCl_2$) at a concentration of 10^6 cells/ml. A volume of 100 μl of the cell solution were labeled with 5 μl FITC Annexin V (BD Pharmingen™) and 5 μl PI (BD Pharmingen). Cells were incubated for 15 min at room temperature (25 °C) in the dark. Subsequently, after the addition of 400 μl of 1X binding buffer, the sample was analyzed by flow cytometry (FACS CANTO II - BD Biosciences) within 1 h. Cell viability is the percentage of live cells in the sample which are characterized by integrity of cellular functions and structure. The double staining with Annexin V and PI by flow cytometry allows to discriminate between cells with high viability which do not bind annexin V and are not co-stained by PI (Annexin V^-/PI^-) as they maintain the integrity of cellular function and structure, cells in early apoptosis (Annexin V^+/PI^-), cells in necrosis (Annexin V^-/PI^+) and cells in late apoptosis (Annexin V^+/PI^+).

2.3. MTT assay

MTT assay was used to colorimetrically evaluate the conversion of MTT (3-[4,5-dimethylthiazol-2-yl]-2,5 diphenyl tetrazolium bromide) into formazan crystals due to the mitochondrial activity of living cells (Corigliano et al., 2018). Cell viability was tested using 12 mM MTT reagent (Sigma-Aldrich, St. Louis, MO) for 2 h at 37 °C. The formazan product was dissolved with 1 mL (12-wells plate) of an organic acid solution (40% dimethylformamide, 2% glacial acetic acid, 16% sodium dodecyl sulfate, pH 4.7), to avoid phenol red interference. The by-products were spectrophotometrically analyzed (at a wavelength of 570 nm), after dissolution in DMSO.

2.4. Pyroelectric sensor design

The pyroelectric sensor is made of a film of PVDF ($\rho = 1.78 \cdot 10^3$ kg/m^3), uniaxially stretched (Measurement Specialties, Hampton, VA, USA). The PVDF film, aluminum metallized on both sides, is covered with a black layer of graphite of 500 nm thick to enhance the absorption of IR radiation. Both additional layers were designed to be much thinner if compared with the PVDF film, to avoid additional heat paths. Uniformly stimulating the PVDF element with an IR radiation to induce a net heat flow between the surfaces of section A, with a heating rate smaller than the thermal diffusivity, a separation of electric charge (or equivalently a generation of an electric potential) $dQ = p_Q A d\theta$ will be induced, where p_Q is the charge-pyroelectric coefficient and θ is the temperature difference between the upper and lower surface. A cylindrical film of PVDF ($r = 0.25$ cm) with a thickness $\tau = 20$ μm is positioned at the bottom of a sample well. On the opposite side, an IR Light Emitting Diode (LED) (OSRAM SFH4550) with a wavelength of 850 nm is fixed at 2 mm from the pyroelectric film, to stimulate pyroelectric response. A charge amplifier topology, converts electric charge into a proportional voltage $V_0 = -Q/C_f e^{(-t/\tau_e)}$, where Q is the electric charge onto the PVDF surfaces and C_f is the feedback capacitance and $\tau_e = R_f C_f$ is the electric time constant of the device (Setiadi et al., 1997; Pullano et al., 2017a,b). Pyroelectric charge is collected through short copper wires ($3 \cdot 10^{-2}$ cm thick). The well has a radius r = 0.25 cm, and a height $H = 0.5$ cm and is designed to be partially filled with 25 μl of sample. From the thermal point of view, the layered structure can be modeled through its respective heat capacity $C_{th} = C_{thS} \cdot C_{thD} / (C_{thS} + C_{thD})$ and thermal conductance $G_{th} = G_{thS} \cdot G_{thD} / (G_{thS} + G_{thD})$, where the subscript S is related to the sample and the subscript D is related to the PVDF film (Fig. 1a). The latter models the heat exchange through conduction and radiation phenomena. In the hypothesis of a homogeneous distribution of the temperature due to the adsorption of the radiant flux distribution, a temperature difference between the lower (T_L) and the upper (T_U) surface of the PVDF is induced (Fig. 1b).

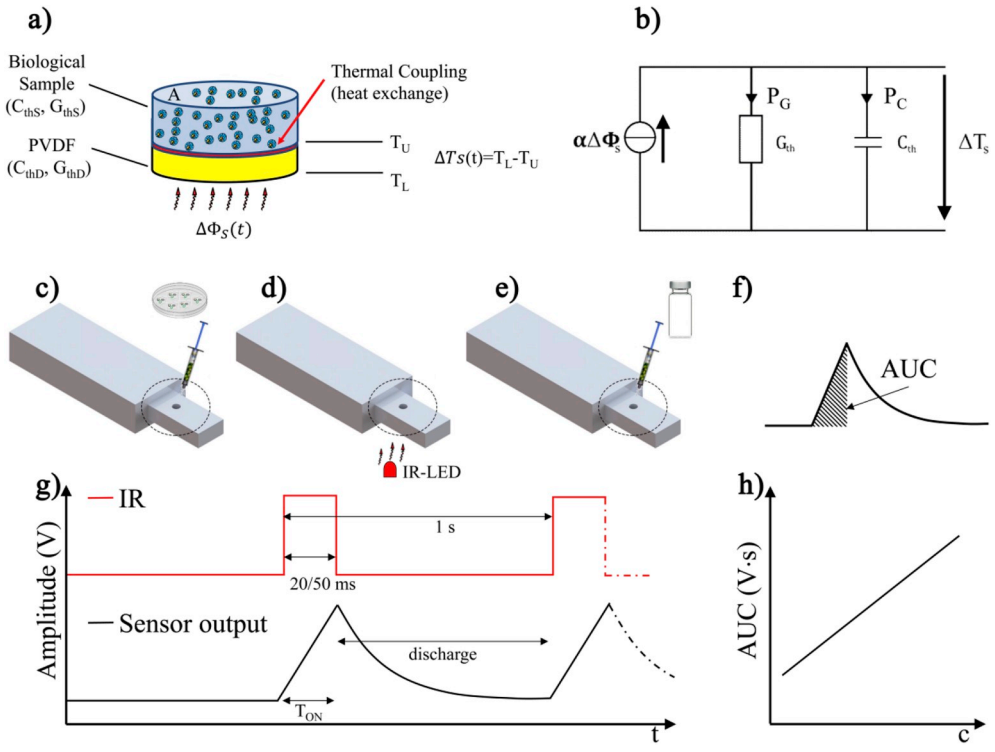

Fig. 1. Representation of the thermal characteristics of the pyroelectric sensor including the IR source, the PVDF, the sample under test, and the thermal coupling among them (a). Equivalent thermal circuit (b). Schematic drawing of the experimental setup procedure. The sample containing the cell population is injected into the well (c). The infrared radiation is activated for a time T_{ON} (d) and after that the sample well is washed with a rinse solution (e). The parameter AUC is evaluated offline (f) by acquiring the pyroelectric sensor output following a specific time sequence (g). A complete dataset is obtained by analyzing cell population at different concentration and/or viability obtaining a bidimensional plot (h).

For a temporally constant radiant flow, the temperature difference across the transducer is correlated to the radiant flux $\Delta\phi$ itself and to the heat exchange modeled with the overall thermal conductance, G_{th}, by:

$$\Delta\theta_S = \frac{\alpha\Delta\Phi_S}{G_{th}} \tag{1}$$

where α is the surface absorption coefficient (Pullano et al., 2014, 2017b). The thermal model of Fig. 1a is characterized by a thermal time constant $\tau_{th} = {G_{th}}^{-1}\cdot C_{th}$ which is a measure of the time response of the pyroelectric sensor while the electric time constant τ_e is introduced by the readout circuit. Both the time constants define the bandwidth of the sensor.

The parameter employed for data comparison is the area under the curve (AUC) defined as the integral of the sensor output voltage in the time interval [t, t + T_{ON}], where T_{ON} is the interval in which the IR radiation beam stimulates the pyroelectric element. The thermal conductance can be related in terms of AUC by combining equations (1) and (2), and considering the output of charge amplifier as follows:

$$G_{th} = -\frac{p_Q A T_{IR}\alpha\Delta\phi}{2C_f AUC} \tag{2}$$

Thermal conductivity is related to the thermal conductance taking into consideration the geometry of the device $k = G_{th}\cdot h/A$, where h corresponds to the height of the cellular suspension into the well. The ratio between the thermal conductivity of a solution k_s, and a continuous matrix k_m, in which spheroids of thermal conductivity k_{cell} are dispersed, can be modeled through the Maxwell model as follows:

$$\frac{k_S}{k_m} = 1 + \frac{3\phi}{\left(\frac{k_{cell}+2k_m}{k_{cell}-k_m}\right)} \tag{3}$$

where ϕ is the volume fraction of the filler. Maxwell model found consistent results if $\phi < 25\%$ (Pietrak and Wisniewski, 2015).

2.5. Thermoelectric measurements

The setup used for thermoelectric measurements is based on the prototype previously described. The prototype is enclosed in a 3D printed case for reducing electromagnetic interferences and providing encapsulation to avoid liquid penetration between the electric part and the sample well. The fluid handling is composed in two main steps: the pipetting of sample into the well and its washing (Fig. 1c–e).

The setup comprises an arbitrary waveform generator (Tektronix AFG3102) and four channels oscilloscope (Tektronix, DPO-3054). Stimulation signal was a unipolar pulse at 1 Hz with a time duration T_{ON} of 20 ms and 50 ms (relative duty cycle of 2%, and 5%, respectively), and an amplitude of 10 V. A 25 µl sample was pipetted into the well and a step-shaped IR beam was transmitted through the sample obtaining the characteristic output signal (Fig. 1g). The experimental setup used for the characterization of liquid droplet cell suspension is depicted in Fig. 2. The sample was first stirred to cause a dispersion of the cells that, being in suspension in the medium, maintain a spheroidal shape to preserve the validity of the Maxwell model (cell aggregation was not considered). A custom software was developed in Matlab (Mathworks) for off-line processing of the dataset and the evaluation of AUC (Fig. 1f–h).

2.6. Experimental procedure

Before experimental analysis, cells were washed in PBS, dissociated using trypsin and resuspended in each specific culture medium. Investigation on IR-induced pyroelectric response was firstly evaluated on highly viable cells at different sample concentrations. From original sample ($8{\cdot}10^3$ cell/µl), a sequence of eight 1:2 serial dilutions were obtained. Concentration of each sample was set to maintain a much lower volume fraction ϕ than the limit of 25% (Pietrak and Wisniewski, 2015). The experiments were performed at 21 °C in a monitored temperature chamber. A sample volume of 25 µl was pipetted into the well and a step-shaped IR beam with a repetition rate of 1 Hz and a duty cycle of 2% and 5% was transmitted through the sample. The pyroelectric activity was recorded using n = 10 subsequent acquisitions.

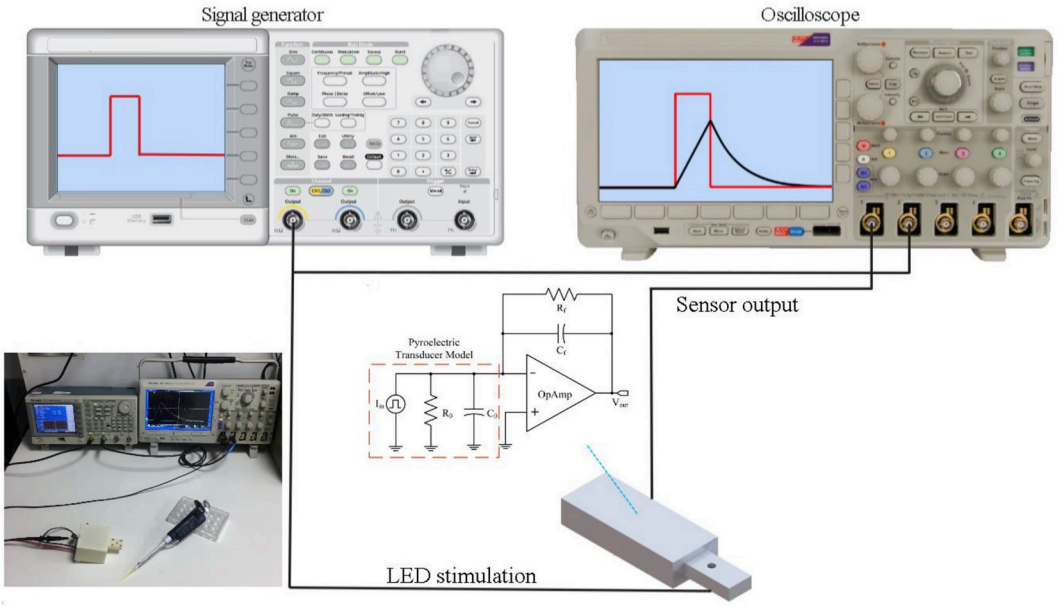

Fig. 2. Overview of the experimental setup used for the characterization of cell suspension and the real implementation (inset).

Off-line AUCs was computed, and data were processed according to each cellular model. After the analysis at different cell concentrations, the effect of viability reduction (i.e. induced necrosis) was investigated. Necrosis was induced by leaving cultured cells at 20 °C for 24h in the absence of CO_2. The contribution in terms of thermal conductivity of cells components (e.g. organelles and cytoplasm), and the role of mitochondrial activity was investigated on HepG2 cells by incubation with Rosiglitazone, an anti-diabetic drug with manifold effects (Costa et al., 2008) and by comparing cell viability with a colorimetric assay (MTT). Finally, apoptosis was investigated on HepG2 cells treated with metformin by flow-cytometry.

2.7. Statistical analysis

Pyroelectric signals were acquired eight times with duplicate samples each time. For all the experiments, data were expressed as mean ± standard deviation. Paired-samples T test were used to compare means of cells thermal conductivities. All statistical analyses were performed by using IBM SPSS 20.0, and a P value < 0,05 was considered statistically significant.

3. Results and discussion

The overall thermal behavior of the system depends on the PVDF thin film and cellular suspension (Fig. 1b). In Table 1 the experimental thermal conductance and heath capacity of PVDF and the estimated parameters for a typical known medium sample are reported.

As evidenced, the estimated thermal conductance of the sample G_{thS} is much smaller than that of the PVDF G_{thD} while the opposite occurs for the heat capacity. Moreover, while the thermal properties of the PVDF, assumed to be constant, maintained unaltered the measurement conditions, the estimated thermal properties of the solution varied due to cellular activity (e.g. inherent thermogenic activity). Following the above-mentioned condition, the induced pyroelectric charge can be related just to the thermal conductance of the sample.

Table 1
THERMAL CHARACTERISTICS OF THE PYROELECTRIC SENSOR AND THE LIQUID SAMPLE.

Heat capacity, C_{thD} (PVDF)	$0.97{\cdot}10^{-3}$ ($J{\cdot}K^{-1}$)
Thermal conductance, G_{thD} (PVDF)	0.195· ($K^{-1}{\cdot}W$)
Est. heat capacity, C_{thS} (Sample)	$\approx 104.65{\cdot}10^{-3}$ ($J{\cdot}K^{-1}$)
Est. thermal conductance, G_{thD} (Sample)	$\approx 9.657{\cdot}10^{-5}$ ($K^{-1}{\cdot}W$)

3.1. Thermal property differences of high-viable cells suspensions

High viability samples have been assessed through the analysis of each of the four cell lines (see Table 1), by a flow cytometer and the double staining with Annexin V and PI.

In Fig. 3, the curves of AUCs vs. concentration evaluated for each cell line at the known concentration are reported. When an IR radiation stimulates a heterogeneous medium whose content is dispersed with positional variability, its propagation inside the medium is different from sample to sample but, in the proposed technique the induced pyroelectric charge is maintained quite linear showing a higher signal variability at lower concentration In fact, in the suspensions investigated, the cells randomly spread out of or disperse. At the lower sample concentrations, the possibility of investigating the contribution of a small population of cells is limited by their random position and inherent temperature fluctuation across the pyroelectric element which is a limiting factor of the resolution of the sensor.

These results have been obtained at T_{ON} = 20 ms (Fig. 3 a, c, e and g) and for T_{ON} = 50 ms (Fig. 3 b, d, f and h). The linearity ranges from R^2 = 0.89 in case of Jurkat up to R^2 = 0.99 in case of HepG2.

The analysis of the pyroelectric–induced effect shows that the response raises as cell concentration increases. According to the thermal model, the increase of AUC by escalating the cellular content in the sample is mainly due to a reduction of thermal conductance and an increase of the heat capacity. The first contribution depends of a higher thermal conductivity due to the presence of more cellular bodies, while building up in heat capacity is mainly due to an increase in cellular mass for a given sample volume. This result evidences how cells characterized by the same viability can be approximated as thermally homogeneous bodies (the position of the constituent elements of the cells is not relevant) dispersed in a homogeneous culture medium. Due to the analysis of the whole sample, the electric charge collected during IR stimulation provides an averaged information about the cell population. More in details, AUC evaluated at both a duty cycle of 2% and 5% evidences a higher linearity at higher sample concentration. Contrarily, when the sample is more diluted inside the culture medium, the positional uncertainty inside the sample increases, thus resulting in a higher random error. A rapid variation in AUC and thus in the thermal

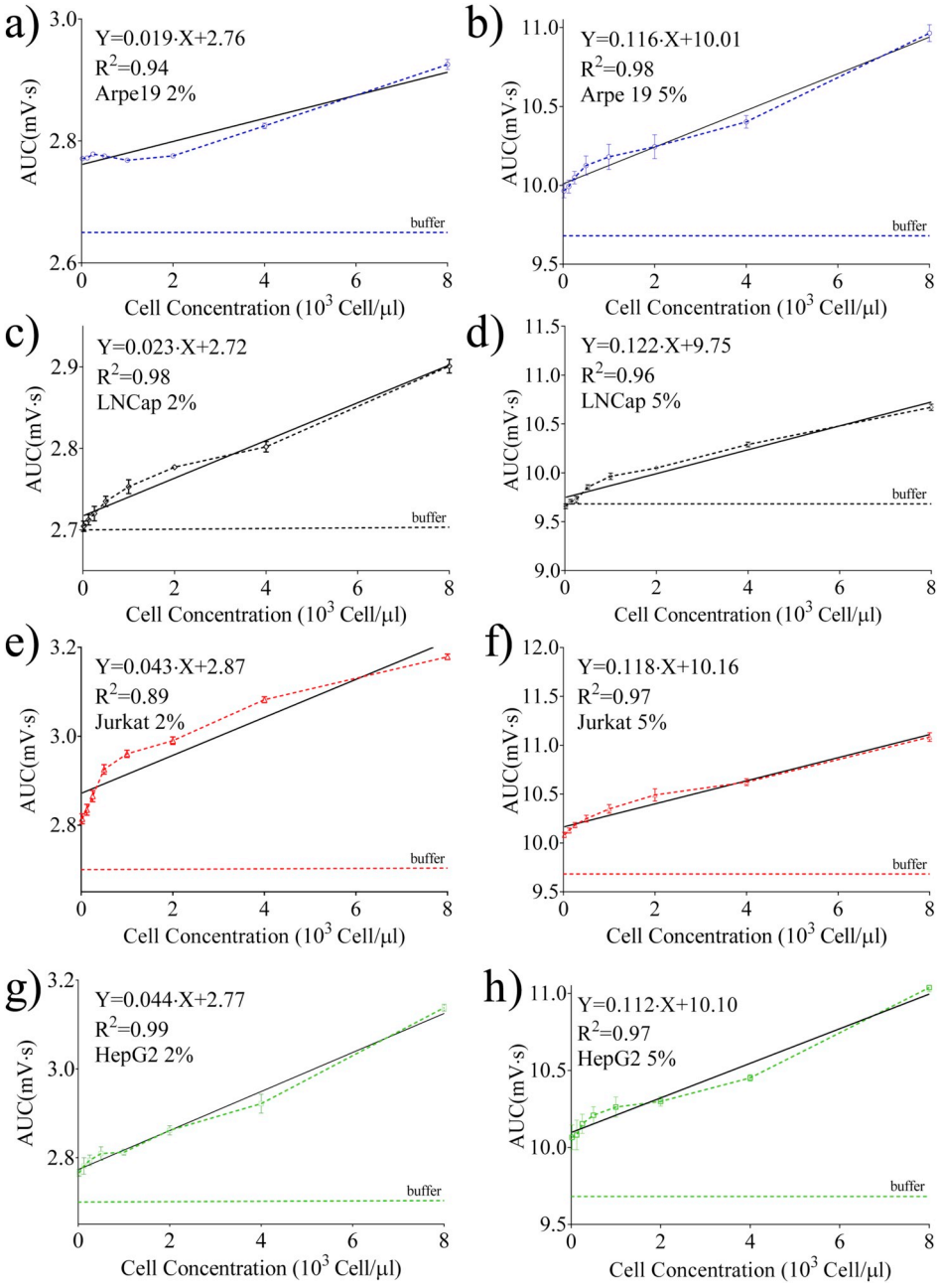

Fig. 3. AUC analysis at few representative concentrations of living cells on raw at a duty cycle of 2% (a, c, e, g) and 5% (b, d, f, h).

characteristics of the solution was observed at lower cell concentration (< 500 cell/µl) followed by steep slope as evidenced in Fig. 3b-h. Even though literature reports very few related-investigations, a similar trend was observed in thermal conductivity of HeLa cell suspension using a different approach (Park et al., 2014). In analogy, rapid variation in thermal characteristics were observed in solution with dispersed particles at a lower volume fraction (Cui et al., 2014). A possible cause of increase was attributed to the distance between cells which decreases as the concentration increases, influencing heat transfer modes (Shayan and Akbari, 2018; Pal and Pal, 2014). Keblinski et al. proposed different possible mechanisms for this anomalous increase in nanofluids which includes Brownian motion of the particles, molecular-level layering of the liquid, the nature of heat transport in the particles, and the effect of clustering (Keblinski et al., 2002). AUC increases as cellular concentration raises, with a slope ranging from $19{\cdot}10^{-3}$ up to $44{\cdot}10^{-3}$ V s·µl·cell^{-1} for T_{ON} = 2% and $112{\cdot}10^{-3}$ up to $122{\cdot}10^{-3}$ V s·µl·cell^{-1} for T_{ON} = 5%. In both cases, the intercept of linear regression approaches a constant value of 2.79 ± 0.07 V s for T_{ON} = 2% and 10.00 ± 0.22 V s for T_{ON} = 5% for RPMI 1640 and of 2.77 ± 0.06 V s for T_{ON} = 2% and 10.01 ± 0.18 V s for T_{ON} = 5% for DMEM F:12. The major source of variability in the AUC coming from the sample can be attributed to agglomeration and settlement characteristics. Average thermal conductivity of each cell line in its respective medium has been evaluated through the Maxwell model, in which the volume fraction ϕ was much lower than the limit of 25% (Pietrak and Wisniewski, 2015). For each concentration, average thermal conductivity of the single cell, k_{cell}, were evaluated for T_{ON} = 2% as showed in Fig. 4c. Average thermal conductivity for alive cells of 0.598 Wm^{-1} K^{-1} for HepG2, 0.601 Wm^{-1} K^{-1} for Jurkat, 0.608 Wm^{-1} K^{-1} for LNCaP and 0.679 Wm^{-1} K^{-1} for Arpe 19 was evaluated. Contrarily to the other cellular models tested, Arpe 19 shows a significantly different thermal conductivity. The reasons can be presumably attributed to the peculiar functional characteristics of the cellular model (Simò et al., 2010). Literature reports that organelles and

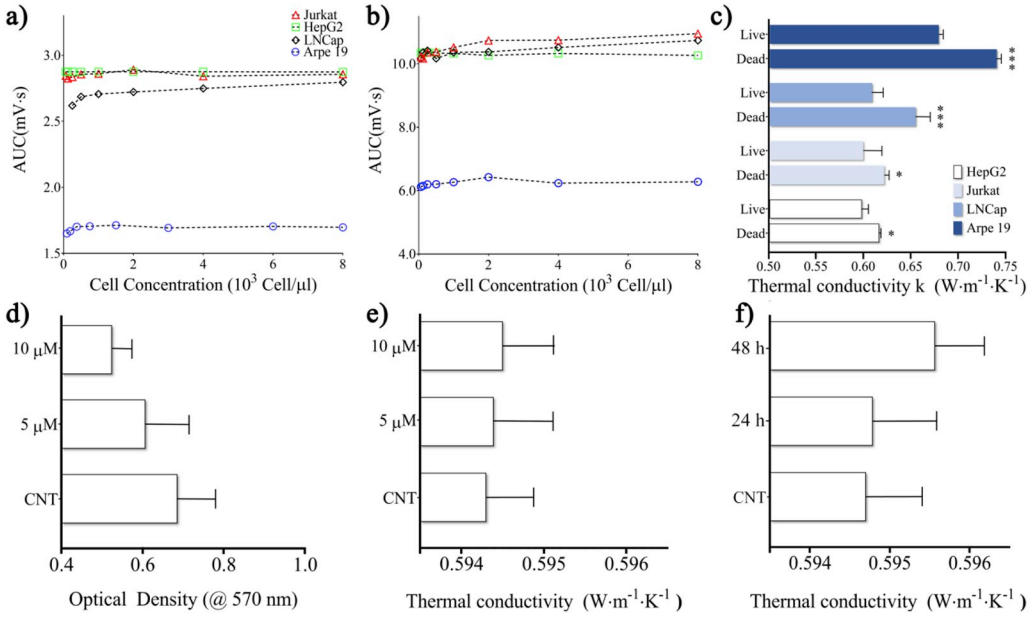

Fig. 4. AUC analysis at a duty cycle of 2% (a) and 5% (b), on necrotic cells. Average thermal conductivities of live and dead cells (c). Comparison of HepG2 cell evaluated by the MTT assay versus Rosiglitazone treatment. Optical density evidenced differences between viability (i.e. mitochondrial activity) of control sample in contrast with samples treated with 5 µM and 10 µM of Rosiglitazone (d). Evaluation of thermal conductivity on the same sample through the induced pyroelectric effect. No significant variation in thermal conductivity was observed (e). Dependence of thermal conductivity on HeG2 cells at 24 h and 48 h after 10 mM Metformin (f).

cytoplasm are characterized by inherent thermal conductivity which ranges from 0.3 up to 0.59 Wm^{-1} K^{-1} (Letfullin et al., 2011). Double lipid layer of cell membrane is characterized by a thermal conductivity that acts as a thermal barrier (Rabin, 2002). However, as the lipid bilayer is characterized by thickness in the nm range, its effect can be considered negligible in the formation of k_{cell}. Thus, the difference in thermal conductivity can be related to the intrinsic properties of each cell line, in relation to the characteristics of the cytoplasm, the nucleus. and the cytosolic organelles, such as mitochondria, ribosomes, etc. (Letfullin et al., 2011).

3.2. Cell viability

Cell death is mainly regulated by non-apoptotic and apoptotic cell death mechanisms. Necrosis is characterized by cellular leakage due to the impairment of cell membrane integrity. Differently, apoptosis is a regulated mechanism characterized by specific changes in cell morphology (e.g. chromatin condensation, nuclear fragmentation, plasma membrane blebbing, and formation of apoptotic bodies) (Liu et al., 2016, Fink and Cookson, 2005). Apoptotic cells precociously expose the membrane phospholipid phosphatidylserine (PS) in the outer side of the plasma membrane. The PS is bound by Annexin V, a Ca^{2+} dependent phospholipid-binding protein. Annexin V may be conjugated to different fluorochromes and represents a sensitive probe for flow cytometric analysis. In Fig. 4a and b the analysis of AUCs versus concentration, after drastic reduction of viability induced by necrosis, is shown. In this condition, mitochondrial activity is limited/absent, and the cell sample is characterized by an abnormal plasma membrane, with leakage of cellular content (Adan et al., 2017). Pyroelectric-induced effect is characterized by an almost constant output without significant variation with cell concentration (Repetto et al., 2008).

As also evidenced in Fig. 4a and b, cells resuspended in RPMI 1640 (i.e. Jurkat, HepG2, LNCaP), showed a response characterized by a lower slope if compared with high viable cells (the effect is influenced by the baseline response of the RPMI1640). Same trend is observed for Arpe19 cells, although it is downshifted, since the culture medium is different (i.e. DMEM F12). This is surprisingly more true even if the cell concentration increases. As results of necrosis, the disintegration of lipid layer and thus the cytoplasm leakage is diluted in the sample medium causing small variations in thermal conductivity of the sample and consequently a constant induced pyroelectric response. The difference in the thermal conductivity between alive and dead cells is statistically significant for all cell lines (HEPG2, Jurkat, LNCaP and ARPE 19, P = 0,037, P = 0,048, P < 0,0001 and P = 0,002, respectively). In all cases the thermal conductivity of dead cells was higher with respect to highly viable counterpart (Fig. 4c). The increase ranges from 2.9% for hepatocytes up to 7.2% in case of prostate cancer cells. There are few evidences in the literature about the thermal conductivity in relation to the death mechanism of a single cell. However, we found agreement with a study conducted by Park et al., in which similar value of k_{cell} for alive and dead hepatocytes were observed using a different approach (Park et al., 2013, 2016). It is noteworthy to highlight that in the case of necrosis or apoptosis at advanced stage, the solution cannot be considered a heterogeneous medium but a homogeneous medium because of the "mixing" between cytoplasm and culture medium. In this case, as expected, the relation between the concentration and the induced pyroelectric activity is quite constant and k_{cell} does not follow Maxwell model. The literature reports few attempts to provide experimental values associated with the thermal component of absorption, (i.e. thermal conductivity). In most cases, the thermal conductivity of the lipid bilayer is correlated to that of fat assuming intracellular contents with an intermediate value between those of the surrounding growth medium and the membrane (Rabin, 2002, Anson and Chivers, 1989). The inhibition of mitochondrial activity and its relationship with thermal conductivity was investigated in HepG2 cell line, and results were compared with flow cytometry, MTT assay and the proposed pyroelectric technique. The inhibition of mitochondrial activity was obtained using Rosiglitazone (a drug of the thiazolidinedione class) at 5 µM and 10 µM. Among the cellular organelles, mitochondria are certainly one of the most important for eukaryotic cells as they perform essential functions for cell survival. The main function, carried out by the mitochondria, is the energetic one. MTT has been assessed for the quantitative evaluation of mitochondrial activity (Fig. 4d). If compared with control, the effect of Rosiglitazone decreases mitochondrial activity, resulting in a reduced optical density of 12% and 25% at 5 µM and 10 µM, respectively. Despite that, no significant variation in thermal conductivity has been observed (i.e. 0.2‰ and 0.16‰) indicating that the mitochondrial activity gives rise to a negligible contribution in the thermal conductivity of a single cell (Fig. 4e).

To investigate whether apoptosis involves differences in thermal conductivity, cells have been treated with metformin. The targets of metformin are manifold. Apart from energy control derived from the regulation of the AMP-activated protein kinase (AMPK), it is implicated in multiple processes, such as apoptosis (Sun et al., 2016). The role of

apoptosis and its implication in thermal conductivity of the cell has been investigated through incubation of HepG2 with metformin at 10 mM. After incubating the cells with metformin (at 24 h 48 h), flow cytometry analysis was performed to evaluate the apoptosis rates and compare them with the control group. In the early stage, the difference between necrosis and apoptosis is that in programmed cell death mechanism plasma membrane excludes PI, and cells will stain with Annexin V only. Thus, differently from necrosis, in the case of apoptosis the integrity of the cells is maintained, and this was investigated to highlight differences in thermal conductivity. Cytofluorimetric analysis of annexin V evidenced that HepG2 treated for 24 h and 48 h with 10 mM of metformin, increases apoptosis rate of 10% and 25%, respectively vs control. In Fig. 4f, the thermal conductivity evaluated in metformin treated cells vs control is reported. Even though cellular integrity is maintained in apoptotic cells, the thermal conductivity of the sample after 48 h is significantly higher than in the control group. This finding suggests the programmed death mechanism involves relevant changes of the intracellular content leading to higher k_{cell}. Moreover, the main contribution of the thermal conductivity can be attributed to the cytoplasm, which in both mechanisms of cell death is characterized by a higher conductivity, as previously reported (Anson and Chivers, 1989). However, additional investigations are required to improve our knowledge on the possible source of change in the response of live cells, compared to that of the dead cells in relation to thermal conductivity for each specific cell line.

3.3. Influence of culture medium and temperature

The contribution of culture mediums onto pyroelectric induced effect was investigated. The baseline level (background at zero concentration) depends on the specific medium in which cells are cultured and resuspended (e.g. higher response for RPMI than DMEM which is due to an inherent lower thermal conductance caused by the different composition of the media). As reported in Fig. 5a the output signal due to the pure medium remains constant over time, even though the same medium from different supply sources showed specific composition which can affect the sensor output differently. The contribution on the sensor output of the temperature drift was evaluated in the range 21–40 °C. The overall system (sensor and electronic unit) has been placed in temperature-controlled chamber with a constant heating rate of 20 °C/h. Wells filled with 25 µl of pure medium (in the proposed case, DMEM F12) were investigated and 8 acquisitions were recorded for each temperature at a duty cycle of 2% (Fig. 5b). Temperature dependence is mainly due to charge amplifier temperature drift, sensor surface thermal radiation and changes in the medium thermal property. The drift of the core operational amplifier of the readout circuit is 2 µV/°C max, and can be easily compensated. However, this could lead to higher AUCs which were not observed instead. Conversely, the contribution due to the thermal radiation results in a decreased net heath flow because the total amount of thermal energy available drops following the thermal radiation law, resulting in a lower induced pyroelectric effect (Pullano et al., 2017a,b). Finally, the effect of evaporation on small volumes of medium will also affect the AUC evaluation leading to higher values as the liquid evaporates. For all these reasons, the overall drift on the output voltage of the device requires to maintain the device at a temperature as constant as possible to avoid temperature drift. PVDF metallization and the absorbing layer plays an important role in the sensor output and need to be considered in the design phase. Both layers were designed to be much thinner if compared with the PVDF film thickness to avoid additional heat paths. For comparison, we investigated the temperature behavior of different upper metal layer (i.e. Aluminum and Silver) with a thickness of 500 nm in contact with pure medium at T_{ON} = 2% with and without the graphite absorbing layer. As shown in Fig. 5b, the lower sensor response was obtained with the bare Silver layer and Aluminum layer. It is mainly due to the different absorption coefficients (α_{Al} = 0.08 and α_{Ag} = 0.04), while the surface emissivity which is involved in the heat transfer by thermal radiation is quite similar between the two layers (δ_{Al} = 0.022, δ_{Ag} = 0.02), (Pullano et al., 2017a,b; MIKRON Instrument Company, 2003; Henninger, 1984). The thin graphite layer in both cases results in an increase of sensor output of about 20%, which is not negligible in the sensor design. In all the cases variations of sensor output are within 5% in the range 21–*40 °C*.

3.4. Additional remarks

One of the weaknesses of the proposed method lies in the composition of the solution and in particular in its susceptibility to be interfered with by the culture media composition, which is especially apparent for label-free assays. Moreover, being in general a mixture of live cells, dead cells and dead cells whose integrity is compromised at an unknown ratio, the thermoelectric analysis results can be affected by random uncertainty. The resuspension of cells in fresh aliquots of culture medium can minimize the errors due to its natural consumption by cells and the contribution of cytoplasmic swelling, irreversible plasma membrane, damage, and organelle breakdown (necrotic cells). Moreover, the use of a differential sensor configuration could make the analysis free from the specific medium used. However, the contribution of dead cells whose integrity is maintained and in general cells inhomogeneity is still a source of error. However, the volume reduction, together with the design of a higher sensitivity electronic interface, can be a feasible way to reduce these errors.

4. Conclusion

We have provided the proof of concept for the *in-vitro* evaluation of the concentration, and indirectly, the average thermal conductivity of a suspended sample of cultured cells using a pyroelectric-based approach.

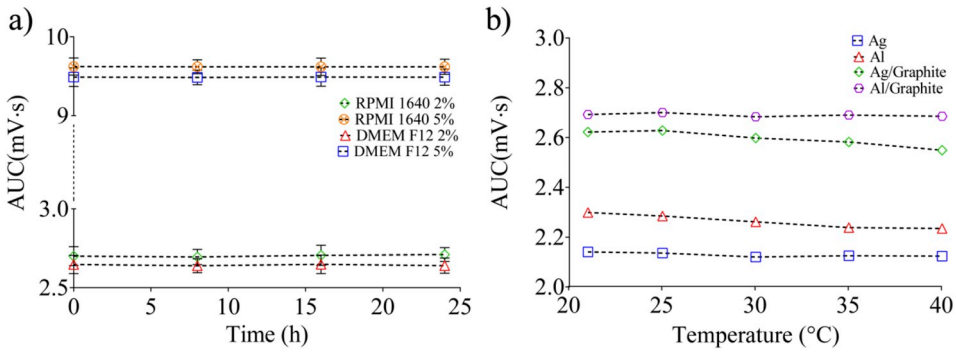

Fig. 5. Effect on the sensor output of plain media in which cells are resuspended and analyzed at a duty cycle of 2% and 5% over 24 h (a), and plain media (RPMI 1640) using different upper PVDF metallizations, carried out at a duty cycle of 2% in the temperature range 21–40 °C (b).

This novel technique of cell characterization can provide a rapid (i.e. real time) analysis to potentially support the cell characterization in terms of viability and concentration, specific for the different cellular model, by a direct correlation of the output voltage of the device with the thermal characteristics of the sample. It results in a label-free and non-invasive technique, with negligible analysis time which can provide quantitative analysis of a sample without any pre-treatment. More importantly, the system can be easily conjugated with electronic devices and integrated in system-on-a-chip for cell culture studies.

CRediT authorship contribution statement

Salvatore A. Pullano: Conceptualization, Methodology, Investigation, Formal analysis, Data curation, Writing - original draft. **Marta Greco:** Validation, Investigation, Formal analysis, Writing - original draft. **Domenica M. Corigliano:** Resources. **Daniela. P. Foti:** Supervision, Writing - review & editing. **A. Brunetti:** Supervision, Writing - review & editing. **Antonino S. Fiorillo:** Supervision, Resources, Visualization, Writing - review & editing.

References

Adan, A., Alizada, G., Kiraz, Y., Baran, Y., Nalbant, A., 2017. Crit. Rev. Biotechnol. 37 (2), 163–176.
Anson, L.W., Chivers, R.C., 1989. Phys. Med. Biol. 34 (9), 1153–1167.
Antoni, D., Burckel, H., Josset, E., Noel, G., 2015. Int. J. Mol. Sci. 16, 5517–5527.
Brunetti, A., Brunetti, L., Foti, D., Accili, D., Goldfine, I.D., 1996. J. Clin. Investig. 97 (1), 258–262.
Chiefari, E., Ventura, V., Capula, C., Randazzo, G., Scorcia, V., Fedele, M., Arcidiacono, B., Nevolo, M.T., Bilotta, F.L., Vitiello, M., Palmieri, C., Gulletta, E., Fusco, A., Foti, D., Vero, R., Brunetti, A., 2016. Sci. Rep. 6, 39426.
Chou, C.-K., Huang, P.-J., Tsou, P.-H., Wei, Y., Lee, H.-H., Wang, Y.-N., Liu, Y.-L., Shi, C., Yeh, H.-C., Kameoka, J., Hung, M.-C., 2018. Biosens. Bioelectron. 117, 97–103.
Corigliano, D.M., Syed, R., Messineo, S., Lupia, A., Patel, R., Reddy, C.V., Dubey, P.K., Colica, C., Amato, R., De Sarro, G., Alcaro, S., Indrasena, A., Brunetti, A., 2018. Peer Journal 8, e5386 2018.
Costa, V., Foti, D., Paonessa, F., Chiefari, E., Pelaia, L., Brunetti, G., Gulletta, E., Fusco, A., Brunetti, A., 2008. Endocrine-Relatd Cancer 15, 325–335.
Cui, W., Shen, Z., Yang, J., Wu, S., Bai, M., 2014. RSC Adv. 4 (98), 55580–55589.
Fink, S.L., Cookson, B.T., 2005. Infect. Immun. 73 (4), 1907–1916.
García-Sánchez, T., Bragós, R., Mir, L.M., 2018. Biosens. Bioelectron. 117, 207–216.
Green, R., Wachsmann-Hogiu, S., 2015. Clin. Lab. Med. 35 (1), 1–10.
Henninger, J.H., 1984. NASA Ref. Pub. 1121Greenbelt. NASA, MD.
Horoszewicz, J.S., Leong, S.S., Kawinski, E., Karr, J.P., Rosenthal, H., Chu, T.M., Mirand, E.A., Murphy, G.P., 1983. Cancer Res. 43 (4), 1809–1818.
Iiritano, S., Chiefari, E., Ventura, V., Arcidiacono, B., Possidente, K., Nocera, A., Nevolo, M.T., Fedele, M., Greco, A., Greco, M., Brunetti, G., Fusco, A., Foti, D., Brunetti, A., 2012. Mol. Endocrinol. 26 (9), 1578–1589.
Keblinski, P., Phillpot, S., Choi, S.U., Eastman, J., 2002. Int. J. Heat Mass Transf. 45 (4), 855–863.
Kucsko, G., Maurer, P.C., Yao, N.Y., Kubo, M., Noh, H.J., Lo, P.K., Park, H., Lukin, M.D., 2013. Nature 500, 54–58.
Letfullin, R.R., Iversen, C.B., George, T.F., 2011. Nanomed. Nanotechnol. Biol. Med. 7, 137–145.
Liu, X., He, J., Liao, C., 2016. Algal. Res. 13, 298–302.
MIKRON Instrument Company, Inc, 2003. Table of Emissivity of Various Surfaces for Infrared Thermometry.
Nicoletti, G., Migliorati, M.C., Pagliacci, F., Grignani, C., Riccardi, C., 1991. J. Immunol. Methods 139 (2), 271–279.
Ongena, K., Das, C., Smith, J.L., Gil, S., Johnston, G., 2010. J. Vis. Exp. 45, 1–5.
Pal, B., Pal, B., 2014. Part. Sci. Technol. 33 (3), 224–228.
Park, B.K., Yi, N., Park, J., Kim, D., 2013. Appl. Phys. Lett. 102 (20), 203702.
Park, B.K., Yi, N., Park, J., Kim, Y., Kim, D., 2014. AIP Adv. 4 (4), 047120.
Park, B.K., Woo, Y., Jeong, D., Park, J., Choi, T.-Y., Simmons, D.P., Ha, J., Kim, D., 2016. J. Appl. Phys. 119 (22), 224701.
Peniuk, G.T., Schnurr, P., Allen, D.G., 2015. J. Appl. Phycol. 28 (1).
Pietrak, K., Wisniewski, T.S., 2015. J. Power. Technol. 95 (1), 14–24.
Pullano, S.A., Islam, S.K., Fiorillo, A.S., 2014. IEEE Sens. J. 14 (8), 2725–2730.
Pullano, S.A., Greco, M., Messineo, S., Brunetti, A., Fiorillo, A.S., 2017a. In: Conference Proceedings on IEEE Sensors.
Pullano, S.A., Mahbub, I., Islam, S.K., Fiorillo, A.S., 2017b. Sensors (Basel) 17.
Pullano, S.A., Greco, M., Corigliano, D.M., Foti, D.P., Brunetti, A., Fiorillo, A.S., 2019. In: Conference Proceedings of the Fourth National Conference on Sensors. pp. 223–228.
Rabin, F., 2002. J. Hyperthermia. 18 (3), 194–202.
Ramirez, T., Stein, N., Aumann, A., Remus, T., Edwards, A., Norman, K.G., Ryan, C., Bader, J.E., Fehr, M., Burleson, F., Foertsch, L., Wang, X., Gerberick, F., Beilstein, P., Hoffmann, S., Mehling, A., van Ravenzwaay, B., Landsiedel, R., 2016. Toxicol. Vitro 32, 278–286.
Repetto, G., del Peso, A., Zurita, J.L., 2008. Nat. Protoc. 3 (7), 1125–1131.
Riccardi, C., Nicoletti, I., 2006. Nat. Protoc. 1, 1458–1461.
Saeys, Y., Van Gassen, S., Lambrecht, B.N., 2016. Nat. Rev. Immunol. 16, 449–462.
Schulten, H.J., 2018. Int. J. Mol. Sci. 19 (10) pii: E2850.
Setiadi, D., Armitage, A., Binnie, T.D., Regtien, P.P.L., Sarro, P.M., 1997. Sensor. Actuator. 61 (1–3), 421–426.
Sharkey, T.D., Schrader, S.M., 2006. High temperature stress. In: Physiology and Molecular Biology of Stress Tolerance in Plants, pp. 101–129.
Shayan, M., Akbari, M.J., 2018. Therm. Anal. Calorim. 134, 2287.
Simò, R., Villarroel, M., Corraliza, L., Hernàndez, C., Ramìrez, M.G., 2010. J. Biomed. Biotechnol. 2010, 190724.
Strober, W., 2015. Curr. Protoc. Im. 111, A3 B.1-A3.B.3.
Sun, Y., Tao, C., Huang, X., He, H., Shi, H., Zhang, Q., Wu, H., 2016. OncoTargets Ther. 9, 2845–2853 2016.
Takahashi, T., 2018. Sci. Rep. 8, 49–67.
Tran, S.L., Puhar, A., Ngo-Camus, M., Ramarao, N., 2011. PLoS One 6 (9) e:22876.
Vega, S., Abian, O., Velazquez-Campoy, A., 2015. Methods 76 (1), 99–115.
Vreugdenburg, T.D., Willis, C.D., Mundy, L., Hiller, J.E., 2013. Breast Canc. Res. Treat. 137, 665–676.
Wang, C., Xu, R., Tian, W., Jiang, X., Cui, Z., Wang, M., Sun, H., Fang, K., Gu, N., 2011. Cell Res. 21, 1517–1519.
Willmer, P., Stone, G., Johnston, I., 2009. Blackwell Publishing, USA.
Xu, X., Xie, X., Duan, Y., Wang, L., Cheng, Z., Cheng, J., 2016. Biosens. Bioelectron. 77 (9), 824–836.
Yasuhiro, K., Motoshi, S., Kenjiro, W., Kazuhiro, F., Takashi, K., Tomonori, D., Yoshihiro, Y., Takeshi, T., Shin, T., Takashi, F., Shunsuke, Y., 2009. Nat. Methods 6, 79–81.
Yu, C., Vykoukal, J., Vykoukal, D.M., Schwartz, J.A., Shi, L., Gascoyne, P.R.C., 2005. IEEE J. Microelectromech. Syst. 14 (3), 480–487.
Zhang, R., Wei, M., Chen, S., Li, G., Zhang, F., Yang, N., Huang, L., 2018. Biosens. Bioelectron. 110, 193–200.